Analysis of guided-resonance-based polarization beam splitting in photonic crystal slabs

Onur Kilic,[1,*] Shanhui Fan,[2] and Olav Solgaard[2]

[1]*Department of Applied Physics, Stanford University, Stanford, California 94305, USA*
[2]*Department of Electrical Engineering, Stanford University, Stanford, California 94305, USA*
[*]*Corresponding author: okilic@stanford.edu*

Received May 23, 2008; accepted August 21, 2008;
posted August 27, 2008 (Doc. ID 96479); published October 10, 2008

We present an analysis of the phase and amplitude responses of guided resonances in a photonic crystal slab. Through this analysis, we obtain the general rules and conditions under which a photonic crystal slab can be employed as a general elliptical polarization beam splitter, separating an incoming beam equally into its two orthogonal constituents, so that half the power is reflected in one polarization state, and half the power is transmitted in the other state. We show that at normal incidence a photonic crystal slab acts as a dual quarter-wave retarder in which the fast and slow axes are switched for reflection and transmission. We also analyze the case where such a structure operates at oblique incidences. As a result we show that the effective dielectric constant of the photonic crystal slab imposes the Brewster angle as a boundary, separating two ranges of angles with different mechanisms of polarization beam splitting. We show that the diattenuation can be tuned from zero to one to make the structure a circular or linear polarization beam splitter. We verify our analytical analysis through finite-difference time-domain simulations and experimental measurements at infrared wavelengths.

OCIS codes: 230.5750, 230.5298, 230.5440.

1. INTRODUCTION

The polarized nature of light can be exploited through the effects of birefringence, dichroism, and optical activity to acquire diverse information such as molecular structure or magnetic field distribution around stars. On the other hand, polarization can be an obstacle in various areas such as interferometry or high-data-rate fiber-optic communication. Both the advantages and disadvantages posed by the polarized nature of light make it essential to have optical components that allow us to manipulate the states of polarization.

One such optical component of interest is the polarizing beam splitter (PBS), a key element in various areas of optics, with applications in optical metrology, optical data storage, optical interconnects, and polarization-based imaging systems. The PBS is also a key element in systems employing polarization entanglement. Some of the applications in this field are in quantum information processing [1] and quantum communication [2].

The most widely used PBSs are prism-based. Such traditional PBSs have limitations in that they provide high polarization extinction ratios only in a narrow range of wavelengths and incidence angles [3]. Form birefringence provides alternative configurations that exhibit better performance [4]. Form birefringence is a type of birefringence that appears due to some geometric anisotropy in an ordinarily nonbirefringent material. If the scale of the anisotropy, such as the spatial period of a grating, is sufficiently small compared to the wavelength, the structure behaves as a homogenous material. The amount of the artificial birefringence can be tuned through several parameters such as geometric composition, material type, and angle of incidence. As a consequence, incident light in two distinct polarizations encounters different effective dielectric constants.

Form birefringence gives the freedom to design diverse polarization-sensitive devices that otherwise would be hard to realize, considering the limited number of available natural birefringent materials. Aside from PBS applications [4–10], form birefringence enables various other devices, including linear polarizers [11], filters [12], lenses [13], and waveplates [14]. Among waveplates, the quarter-wave retarder (QWR) is an optical component of special interest in this paper. QWRs are used for polarization analysis and control, usually employed as a linear-to-circular—or *vice versa*—polarization transformer. Form birefringence can be employed to create various types of QWRs with advantages over traditional types [7,14–18].

By using a QWR together with a PBS, one can construct a circular PBS. Several circular PBSs utilizing liquid crystals were reported in the past, based on chiral media [19] and polarization diffraction gratings [20]. Azzam and Mahmoud demonstrated such a beam splitter based on conventional thin-film optics [21]. Their structure, which is a dual-QWR that induces quarter-wave retardation of opposite sign for the reflected and transmitted waves, has as its basis a self-supporting trilayer pellicle. The limitation of this structure is its operation at a high angle of incidence and unequal power in the reflected and transmitted beams. These limitations were overcome in a later device by Azzam and De by embedding the trilayer pellicle in a high-index prism and operating it under frustrated-total-internal-reflection conditions [22].

Here we analyze structures based on photonic-crystal slabs (PCS) that act as unique polarization components. Photonic-crystal-based polarization elements have been

investigated in the past, such as bulk 2D-photonic-crystal-based PBSs [23] and QWRs [24]. Lousse *et al.* reported simulations of a linear PBS based on a PCS with rectangular holes [25]. The PCS structure we describe here acts as a dual-QWR, where the fast and slow axes are switched for reflection and transmission. The operation of the structure relies on the phase and amplitude responses of guided resonances [26–34]. An incoming wave linearly, circularly, or elliptically polarized and incident on such a structure is split into two orthogonal polarization modes, each sharing half the incident power. The diattenuation, defined as the difference in the transmitted powers for the two polarizations normalized to the total transmitted power, can be tuned from zero to one to make the structure a circular or linear PBS. By introducing a small amount of form birefringence into the photonic crystal geometry, the structure can perform at normal incidence, opening up the novel applications discussed in Section 6.

2. PHASE AND AMPLITUDE RESPONSE OF BIREFRINGENT PCS

For light incident on a PCS (as illustrated in Fig. 1), the transmission coefficient t and the reflection coefficient r can be expressed as [29,30]

$$t = t_d - (t_d \pm r_d)\gamma/[\gamma + j(\omega - \omega_0)],$$

$$r = r_d - (r_d \pm t_d)\gamma/[\gamma + j(\omega - \omega_0)]. \quad (1)$$

Here the parameters γ and ω_0 are the half-linewidths and center frequencies of the guided resonances, respectively and $\pm$ corresponds to even and odd modes with respect to the mirror plane parallel to the slab. Throughout the text the upper sign will correspond to even modes and the lower sign to odd modes.

The parameters t_d and r_d are the direct transmission and reflection coefficients. They can be expressed as the transmission and reflection coefficients of an equivalent uniform slab of the appropriate effective refractive index. At normal incidence, they are [35]

$$t_d = \left[\cos(k_z h) - j\frac{k_{z0}^2 + k_z^2}{2k_{z0}k_z}\sin(k_z h)\right]^{-1},$$

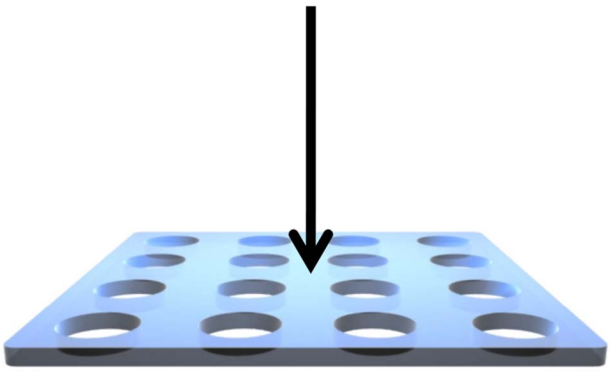

Fig. 1. (Color online) Illustration showing light normally incident on a PCS.

$$r_d = \left[j\frac{k_{z0}^2 - k_z^2}{2k_{z0}k_z}\sin(k_z h)\right]t_d, \quad (2)$$

where $k_{z0} = (\omega/c)\sqrt{\epsilon_0}$ and $k_z = (\omega/c)\sqrt{\epsilon}$ represent the wave vector components normal to the slab, and h is the thickness of the slab. The PCS is surrounded by a medium with a dielectric constant of ϵ_0 (usually air/vacuum with $\epsilon_0 = 1$), while ϵ is the frequency-dependent dielectric constant, found by fitting the above expressions to the Fabry–Perot type background of the PCS transmission and reflection spectra [29].

For compactness, we introduce the parameters α and β that we will refer to as the normalized frequency offset and the splitting ratio, respectively:

$$\alpha(\omega) = (\omega - \omega_0)/\gamma,$$

$$\beta(\omega) = \frac{k_{z0}^2 - k_z^2}{2k_{z0}k_z}\sin(k_z h). \quad (3)$$

The splitting ratio β, a real number, is the ratio between the direct reflection and transmission due to $r_d = j\beta t_d$.

Now let us consider the case where we have birefringence in the PCS, so that for the two orthogonal eigenpolarization axes 1 and 2, we have in general different transmission coefficients $t_1 \neq t_2$. To achieve this, the guided resonances corresponding to the polarizations 1 and 2 must be split by Δ from the center frequency ω_0 into the positive and negative frequency directions. We can understand the conditions for the existence of such a pair of resonances through symmetry considerations. Let us consider the case for a square-lattice PCS. At the Γ point (referring to a zero value of the wave vector component parallel to the slab), the structure possesses a C_{4v} point group symmetry in the plane of the lattice, together with the even/odd symmetry with respect to the mirror plane parallel to the slab (a C_{1h} symmetry). The C_{4v} point group supports five classes of eigenmodes belonging to different irreducible representations and hence possess different spatial symmetry. Among these five classes, one of them is doubly degenerate. Symmetry matching conditions permit only the doubly degenerate modes to couple to outside plane-wave radiation that is normally incident on the slab [36]. Consequently, for our case of normal incidence, the guided resonances are always doubly degenerate in a square lattice. When we introduce a small form birefringence into the lattice by either making the holes slightly elliptical, or by slightly varying the pitch in one direction, we break the 90° rotational symmetry. As a result the symmetry of the lattice is reduced to a C_{2v} symmetry. The C_{2v} point group does not support degenerate modes. Therefore the modes that are degenerate in the square lattice split into two different modes when we introduce a small form birefringence, with the magnitude of the splitting determined by the amount of the asymmetry introduced. The uncoupled modes that are nondegenerate in the square lattice remain uncoupled for the form-birefringent case also, so that all guided resonances appear as a pair of split modes.

As we introduce a small form birefringence into the PCS, the other parameters defining the resonances, which are the background and linewidth, can also deviate

for the two polarizations. A change in these parameters that affects both polarizations similarly is not significant to our analysis. We will see that we can neglect any deviation in the background and linewidth for the two polarizations, and also can ignore any change in them. The background will not be affected much, since it is mainly a function of the effective dielectric constant of the corresponding uniform slab. If we introduce the form birefringence in such a way that we do not change the average dielectric constant, then the background will not vary significantly for either polarization. (The method is also described in Appendix A.) This argument is supported by the finite-difference time-domain (FDTD) simulations shown in Fig. 2. The simulations were done for a dielectric slab with a dielectric constant of 12 and a thickness of $0.55a$, a being the lattice constant of rectangular through holes on a square lattice. A simulation was first done for square-shaped holes of size $0.5a \times 0.5a$. Then we calculated the splitting ratio β at the frequency $\omega = 0.3(2\pi c/a)$, where it is expected to have a value of 0. Subsequently we made a series of calculations in which the widths of the rectangular holes were gradually increased (along the direction 2) by keeping the area of the holes $(0.5a \times 0.5a)$ constant, so that the holes became increasingly rectangular. A hole width of $0.5a$ corresponds to square holes, while a hole width of $1.0a$ corresponds to a 1D grating, since the rectangular holes become connected when their width is equal to the lattice constant. The β values at the frequency $\omega = 0.3(2\pi c/a)$ for the two polarizations were calculated for increasing form birefringence.

The result shows that even for a very large form birefringence, where the structure becomes a 1D grating, the change in β is not large. The splitting ratio for polarization 1 (β_1) stays nominally the same, while the splitting ratio for polarization 2 (β_2) changes by 0.2, which is only 6.25% of the maximum range of β values for a slab with a dielectric constant of 12. This supports our argument that the background does not change significantly for a small birefringence.

The guided resonances, on the other hand, are strongly affected by any geometrical variation such as changing the radius of the holes or the pitch. Since the introduction of form birefringence is equivalent to a change in the lattice geometry, we expect both the center frequencies and the linewidths of the individual resonances to change when splitting occurs. Numerical simulations (as presented in Fig. 3) show that the relative changes for the resonance frequency and linewidth of a guided resonance are of the same order, i.e., $d\omega/\omega \approx d\gamma/\gamma$. However, in our case we are interested in the changes of center frequency and linewidth relative to the linewidth. This is because we are interested in how far apart the resonances are, and how much they overlap in comparison to the linewidth, irrespective of the center frequency. In that case, the relative change in the center frequency would be $d\omega/\gamma = (\omega/\gamma)d\omega/\omega = (\omega/\gamma)d\gamma/\gamma$. This means that the change in the center frequency is larger than the change in the linewidth by a factor of the order of ω_0/γ. This number corresponds to Q, the quality factor of the guided resonance. Q values for guided resonances typically vary from ~100 to ~5000 [29]. This in turn means that the linewidth does not change significantly when the doubly degenerate resonances split.

These arguments are supported by the FDTD simulations shown in Fig. 3. The simulations show that the linewidth does not change significantly when the doubly degenerate resonances split. The guided resonances used in the calculations were isolated from the background spectrum by passing the complex field amplitude through a

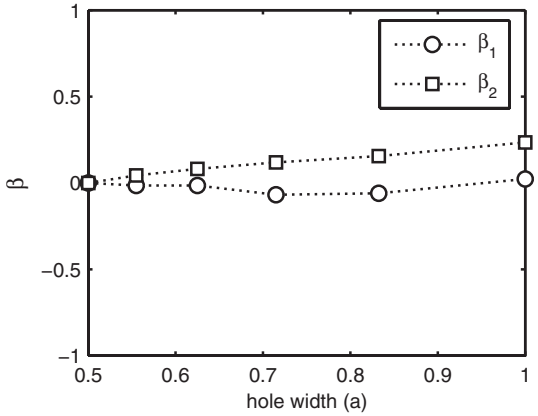

Fig. 2. FDTD simulations showing that the background is not significantly affected by an introduction of a form birefringence. The simulations were done for a dielectric slab with a dielectric constant of 12 and a thickness of $0.55a$, a being the lattice constant of rectangular through holes on a square lattice. A simulation was first done for square-shaped holes of size $0.5a \times 0.5a$. Then, the β value at the frequency $\omega = 0.3(2\pi c/a)$ was calculated, where it has a value of 0. Afterward, the width of the rectangular holes was gradually increased (along the direction 2) by keeping the area of the hole $(0.5a \times 0.5a)$ constant. The horizontal axis corresponds to the hole width. The hole width of $0.5a$ corresponds to square-shaped holes, while the hole width of $1.0a$ corresponds to a 1-D grating, since the rectangular holes become connected. The rectangular and circular data points correspond to the β values at the frequency $\omega = 0.3(2\pi c/a)$ for the two polarizations.

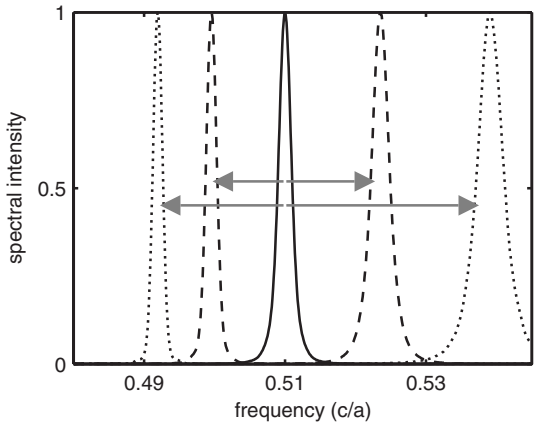

Fig. 3. FDTD simulations showing that the linewidth does not change significantly when the doubly degenerate resonances split. The data are from the same simulations that are used in Fig. 2. The graph shows how a guided resonance splits through form birefringence. The solid curve corresponds to a doubly degenerate resonance for a hole width of $0.5a$, which is a square hole. By introducing birefringence through making the holes rectangular, the doubly degenerate resonance splits into two. The dashed curves correspond to split resonances for a hole width of $0.55a$, and the dotted curves correspond to split resonances for a hole width of $0.63a$. The guided resonances used in the calculations were isolated from the background spectrum by passing the complex field amplitude through a high-pass filter.

high-pass filter. The data are from the same simulations used to calculate the background change in Fig. 2. The graph shows how a guided resonance splits through form birefringence. First there is a doubly degenerate resonance for a hole width of $0.5a$, i.e., a square hole. By introducing birefringence (by making the holes rectangular and keeping their area constant as described before), the doubly degenerate resonance splits into two.

The simulations were done for form-birefringent PCS structures where hole widths were $0.55a$ and $0.63a$. The ratio of the center frequency difference to the linewidth difference is $\Delta\omega/\Delta\gamma=34$ and 24 for the hole widths $0.55a$ and $0.63a$, respectively. These numbers show that the change in frequency is larger than the change in linewidth by more than an order of magnitude. For a small birefringence, this number would be closer to the Q value of the original PCS resonance, which is 222. This example shows that even for such a small Q, our argument that the frequency changes faster than the linewidth holds.

We have to note that these statements are not valid for very small hole radii. In the limit where the hole radius approaches zero the Q values for the resonances diverge, since the resonances become true guided modes in a uniform slab [29]. The normalized frequency offsets for the two polarizations can be written symmetrically as

$$\alpha_1(\omega) = [\omega - (\omega_0 - \Delta)]/\gamma,$$

$$\alpha_2(\omega) = [\omega - (\omega_0 + \Delta)]/\gamma, \tag{4}$$

where ω_0 corresponds now to the mean of the center frequencies of the two guided resonances. The transmission coefficients are then simply

$$t_{1,2} = t_d - (t_d \pm r_d)/(1 + j\alpha_{1,2}). \tag{5}$$

By writing the direct reflection coefficient in the form $r_d = j\beta t_d$, the transmission coefficient can be put into the compact form

$$t = t_d(j + \alpha)(\alpha \mp \beta)/(1 + \alpha^2). \tag{6}$$

The induced phase difference [37] between the transmitted polarizations 1 and 2, namely the retardance, will then be, using Eq. (6),

$$\Delta\Phi_t = \arg(t_2/t_1) = \arg\left(\frac{j + \alpha_2}{j + \alpha_1}\right) + \arg\left(\frac{\alpha_2 \mp \beta}{\alpha_1 \mp \beta}\right). \tag{7}$$

We will use the abbreviation $\arg[(j+\alpha_2)/(j+\alpha_1)]=\Phi_0$ to denote the retardance due to the guided resonance splitting. We see that the total retardance $\Delta\Phi_t$ can have an additional phase contribution of π due to interference with the background, when the phase parameter $(\alpha_2 \mp \beta)(\alpha_1 \mp \beta) = \rho_t$ is negative. In fact, we will exploit this additional phase to make a PBS out of a PCS. We are going to use the phase parameter ρ, together with the normalized frequency offset α and the splitting ratio β, to determine all the relevant PBS properties of a PCS.

By rewriting the retardance with those abbreviations we obtain the compact form

$$\Delta\Phi_t = \begin{cases} \Phi_0 & \rho_t \geq 0 \\ \Phi_0 + \pi & \rho_t < 0 \end{cases}. \tag{8}$$

Similarly for the reflected wave, where the phase parameter is $\rho_r = (1 \pm \beta\alpha_2)(1 \pm \beta\alpha_1)$, we get the retardance as

$$\Delta\Phi_r = \begin{cases} \Phi_0 & \rho_r \geq 0 \\ \Phi_0 + \pi & \rho_r < 0 \end{cases}. \tag{9}$$

Having found the phase responses for a birefringent PCS, let us now find the amplitude responses for the polarizations 1 and 2. Using the expression $|t_d|^2 + |r_d|^2 = 1$, together with Eq. (6), we get the transmittance in the explicit form

$$|t_{1,2}|^2 = (\alpha_{1,2} \mp \beta)^2/[(1 + \beta^2)(1 + \alpha_{1,2}^2)]. \tag{10}$$

Combining this result with $|t|^2 + |r|^2 = 1$, we find the reflectance in the explicit form

$$|r_{1,2}|^2 = (1 \pm \beta\alpha_{1,2})^2/[(1 + \beta^2)(1 + \alpha_{1,2}^2)]. \tag{11}$$

We are using the energy conservation expressions $|t_d|^2 + |r_d|^2 = 1$, and $|t|^2 + |r|^2 = 1$ under the assumption that there is no absorption in the PCS. This is a good assumption for most PCS types, such as silicon-based ones operating at infrared wavelengths.

Equations (10) and (11) provide expressions for the transmittance and reflectance in terms of the normalized frequency offset α and the splitting ratio β. We are going to employ these expressions in Section 3 to analyze the conditions under which a PCS acts as a PBS that separates an incoming elliptical beam equally into its orthogonal constituents.

3. POLARIZATION BEAM SPLITTING AT NORMAL INCIDENCE

In this section we will analyze how we can employ a PCS as a PBS at normal incidence. The Jones formalism offers practical advantages when analyzing polarization properties. Omitting arbitrary phases, the Jones matrices for transmission and reflection can be written as

$$J_t = \begin{bmatrix} |t_1| & 0 \\ 0 & |t_2|e^{j\Delta\Phi_t} \end{bmatrix}, \quad J_r = \begin{bmatrix} |r_1| & 0 \\ 0 & |r_2|e^{j\Delta\Phi_r} \end{bmatrix}. \tag{12}$$

For an incident wave $|i\rangle$ the transmitted and reflected waves will be $|t\rangle = J_t|i\rangle$ and $|r\rangle = J_r|i\rangle$, respectively. By choosing an appropriate coordinate system (i.e., choosing an appropriate relative orientation between the eigenpolarization axes of the PCS and the incident wave), any wave with a definite polarization can be put into the form

$$|i\rangle = \frac{1}{\sqrt{2}}\begin{bmatrix} 1 \\ e^{j\delta} \end{bmatrix}. \tag{13}$$

This denotes a general elliptical polarized wave ($\mathcal{E}$ state) with a polarization phase δ that defines the ellipticity. The special polarization states for this choice of coordinate system are plane-polarized at ±45° (±45° $\mathcal{P}$ state), circular-right polarized ($\mathcal{R}$ state), and circular-left polarized ($\mathcal{L}$ state).

For the PCS to be capable of separating an incoming beam equally into two orthogonal constituents (any two orthogonal elliptical polarization states, such as two linear ones, or circularly polarized states) the first conditions for a PBS are the amplitude conditions $\langle t|t\rangle = \langle i|J_t^\dagger J_t|i\rangle = 1/2$ and $\langle r|r\rangle = \langle i|J_r^\dagger J_r|i\rangle = 1/2$, which we can express through a trace (denoted with the symbol Tr) simply as

$$\mathrm{Tr}(J_t^\dagger J_t) = \mathrm{Tr}(J_r^\dagger J_r) = 1. \tag{14}$$

This means that for a general $\mathcal{E}$ state, the incoming wave is separated into two equal parts, so that half the power is reflected in one state and half the power is transmitted in the other state. To satisfy Eq. (14), we need to have $|t_1|^2 + |t_2|^2 = |r_1|^2 + |r_2|^2 = 1$. Using the energy conservation $|t|^2 + |r|^2 = 1$, this can be expressed as $|t_1| = |r_2|$ and $|t_2| = |r_1|$, which means that the phase parameters for reflection and transmission are related through

$$\frac{\rho_r^2}{\rho_t^2} = \frac{|r_1|^2}{|t_2|^2}\frac{|r_2|^2}{|t_1|^2} = 1, \tag{15}$$

leading us to the two solutions

$$\rho_r = -\rho_t, \quad \rho_r = +\rho_t. \tag{16}$$

The second condition for a PBS is that the reflected and transmitted parts have orthogonal polarizations $\langle t|r\rangle = \langle i|J_t^\dagger J_r|i\rangle = 0$, which can be expressed as

$$\mathrm{Tr}(J_t^\dagger J_r) = 0. \tag{17}$$

Using $|t_1| = |r_2|$ and $|t_2| = |r_1|$ in Eq. (17), we see that for orthogonality we just need to have $\Delta\Phi_r - \Delta\Phi_t = \arg(\rho_r/\rho_t) = \pi$. This means that the orthogonality condition is $\rho_t/\rho_r < 0$. Hence, the solution in Eq. (16) that satisfies both the amplitude and orthogonality conditions is $\rho_t = -\rho_r$. This condition is satisfied for $\alpha_1 = -1/\alpha_2$, so the PCS operates as a PBS at normal incidence if $\alpha_1\alpha_2 = -1$. When we solve $\alpha_1\alpha_2 = -1$ for the frequency ω, we obtain the two results

$$\omega^{(1)} = \omega_0 - \sqrt{\Delta^2 - \gamma^2},$$

$$\omega^{(2)} = \omega_0 + \sqrt{\Delta^2 - \gamma^2}. \tag{18}$$

At these frequencies, the reflected and transmitted beams will have orthogonal polarizations and equal power. We first note the interesting result that the PBS frequencies are independent of the background and depend solely on the normalized frequency offsets. We also observe that the splitting has to be at least a linewidth wide $\Delta \geqslant \gamma$ to enable PBS operation. There are also trivial solutions to the two PBS conditions—either $|t_1| = |r_2| = 0$ or $|t_2| = |r_1| = 0$—which correspond to a linear PBS for which we have no power in one eigenpolarization for reflection and transmission. In that case the retardances $\Delta\Phi_t$ and $\Delta\Phi_r$ are undefined, hence have no physical meaning. However, if we look at frequencies slightly smaller and larger than ω_0 we have nonvanishing power in both polarizations, and hence definite retardances. In fact, we have $\Delta\Phi_r - \Delta\Phi_t = \pi$ for the limiting cases of $\omega \to \omega_0^+$ and $\omega \to \omega_0^-$, as can be seen from the retardances shown in Fig. 4.

The retardance due to the guided resonance splitting Φ_0 will have the value of $\pi/2$ for $\alpha_1\alpha_2 = -1$. Since the relation between the phase parameters for transmission and reflection in this case will be $\rho_t/\rho_r = -1$, the retardances will be $\Delta\Phi_t = +\pi/2$ and $\Delta\Phi_r = -\pi/2$ for a positive phase parameter $\rho_t > 0$. Similarly for $\rho_t < 0$, we will have $\Delta\Phi_t = -\pi/2$, and $\Delta\Phi_r = +\pi/2$. The Jones matrices for transmission and reflection will then be (for concreteness we show the $\rho_t > 0$ case; for the $\rho_t < 0$ case, replace j by $-j$)

$$J_t = \begin{bmatrix} |t_1| & 0 \\ 0 & j|t_2| \end{bmatrix}, \quad J_r = \begin{bmatrix} j|t_2| & 0 \\ 0 & |t_1| \end{bmatrix}. \tag{19}$$

These matrices emphasize an interesting feature: the structure acts as a retarder for which the fast and slow axes are switched for transmission and reflection. This means that for a general $\mathcal{E}$ state, the incoming wave is

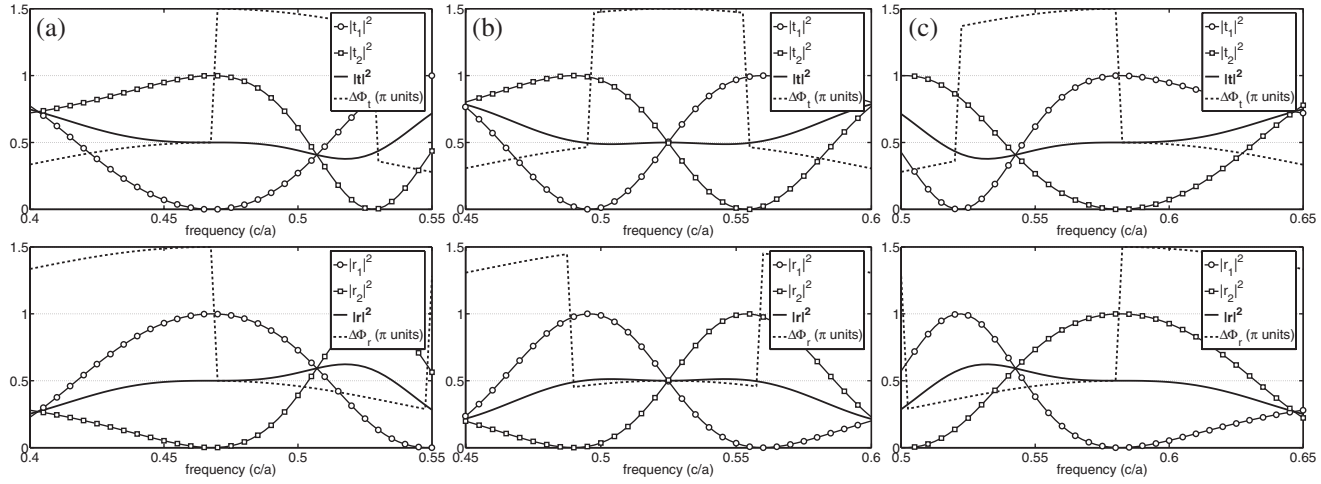

Fig. 4. Calculated spectra of the phase and amplitude responses for transmission (top) and reflection (bottom) for three different form-birefringent PCS structures (a), (b), and (c). The circle-marked, square-marked, and solid curves correspond to the normalized powers in polarization 1, polarization 2, and both polarizations, respectively. The dashed line corresponds to the retardance in units of π. The structure has a dielectric constant of 12 with a thickness of $0.55a$, a being the pitch. The guided resonances possess a half-linewidth of $\gamma = 0.064(2\pi c/a)$, are separated by $\Delta = \gamma$, and have $\omega^{(1)} = \omega^{(2)} = \omega_0$ values of $0.47(2\pi c/a)$, $0.53(2\pi c/a)$, and $0.58(2\pi c/a)$ for the cases (a), (b), and (c), respectively. (a) corresponds to a linear PBS with $\beta = -1$, (b) to a circular PBS with $\beta = 0$, and (c) to a linear PBS with $\beta = +1$, in the same way as it is illustrated in Fig. 5.

Table 1. Special Values of the Splitting Ratio β and the Corresponding Values of the Amplitudes $|t_1|$ and $|t_2|$[a]

	Even Modes			Odd Modes		
β	−1	0	1	−1	0	1
$\lvert t_1\rvert$	0	$1/\sqrt{2}$	1	1	$1/\sqrt{2}$	0
$\lvert t_2\rvert$	1	$1/\sqrt{2}$	0	0	$1/\sqrt{2}$	1

[a]These numbers determine whether the PCS acts as a linear, circular, or any other kind of elliptical PBS.

separated into its two orthogonal constituents at $\omega=\omega^{(1)}$ or $\omega^{(2)}$, so that half the power is reflected in one state, and half the power is transmitted in the other state. The composition of the Jones matrix is dependent on the amplitudes $|t_1|$ and $|t_2|$, which because of Eq. (10) is dependent on the splitting ratio β at the operation frequency of $\omega=\omega^{(1)}$ or $\omega^{(2)}$. The cases for special β values are listed in Table 1 corresponding to different diattenuation values.

The implication of Table 1 is illustrated in the examples in Fig. 5. Calculated transmission and reflection spectra corresponding to those examples, together with the retardances, are shown in Fig. 4. The calculations were carried out by directly using the basic expressions in Eqs. (1) and (2) for the case when the splitting is equal to the linewidth $\Delta=\gamma$, so that we have $\omega^{(1)}=\omega^{(2)}=\omega_0$. The dielectric constant in the calculations is fixed at 12 for simplicity, so that it does not vary with frequency. The slab thickness is chosen as $h=0.55a$. The resonances are due to even modes for concreteness. The half-linewidth for all cases is $\gamma=0.064$ $(2\pi c/a)$. The center frequency ω_0 is chosen to be 0.47, 0.53, and 0.58 $(2\pi c/a)$, so that at $\omega=\omega_0$ we have the three interesting cases of $\beta=-1$, $\beta=0$, and $\beta=+1$, respectively. The calculated spectra clearly verify our analysis of the amplitude and phase responses. We see that the incident power is equally separated through transmission and reflection into orthogonally polarized light.

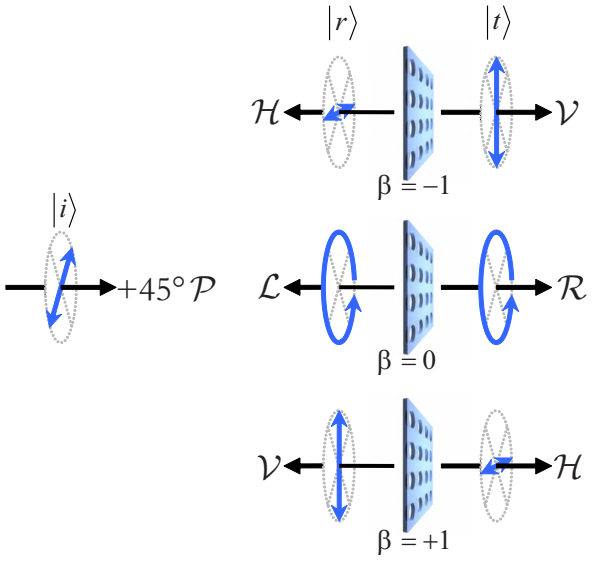

Fig. 5. (Color online) Illustration showing how the PCS-based PBS operates for several special β values.

The least dispersive solution, which is desirable for most applications where chromaticity is a disadvantage, is for the case when the splitting is equal to the linewidth, $\Delta=\gamma$. In such a case, the PBS operates at a single frequency $\omega^{(1)}=\omega^{(2)}=\omega_0$, which is the center frequency. Figure 6 shows the operation of the PBS on the Poincaré sphere for several cases, such as a gradual change in the splitting ratio or the incident polarization, including situations when the incident beam is not aligned to the eigenpolarization axes of the PBS.

4. POLARIZATION BEAM SPLITTING AT OBLIQUE INCIDENCE

In the previous section, we demonstrated that a PCS can act as a PBS if two guided resonances corresponding to orthogonal polarizations are separated by more than the linewidth. Besides introducing a small form birefringence and striking with light at a normal angle, there is another way to separate two guided resonances and hence construct a PBS out of a PCS. When we move out of the Γ point (so that we have a nonvanishing wave vector component parallel to the slab), the symmetry of the lattice is reduced. Consequently, the modes that are doubly degenerate at normal incidence appear to be split at an oblique incidence angle, as in the case of introducing form birefringence to reduce the C_{4v} symmetry to a C_{2v} symmetry. Particularly, the symmetry in the case of a finite wave vector component parallel to the slab is in general lower than C_{2v}. As a result, nondegenerate modes that are uncoupled in the Γ point begin to become coupled to the incident radiation for increasing incidence angles. [25,36] These additional modes can contribute to more complex polarization effects at oblique incidences that we are not going to discuss in this paper. In the case of oblique incidence (as illustrated in Fig. 7), we then do not need any form birefringence to split the resonances. We need to note that any presence of a form birefringence is not an obstruction, though; it is only not a requirement, and can, in fact, be used to control the splitting at oblique incidences. The fact that the backgrounds for the two polarizations have a different behavior for increasing angles of incidence is taken into account in the following analysis. This is in contrast with the normal-incidence case where there is no significant difference between the backgrounds for the two polarizations. The statement that $d\omega_0/\gamma$ is in general significantly larger than $d\gamma/\gamma$ is also valid for splitting through increasing incidence angles (as can be seen, e.g., from the FDTD simulations in [25]).

For the more general case of incidence at an oblique angle, the direct transmission and reflection coefficients for the s and p polarizations (which we will denote with the indices 1 and 2 for consistency) are [35]

$$t_{d1}=\left[\cos(k_z h)-j\frac{k_{z0}^2+k_z^2}{2k_{z0}k_z}\sin(k_z h)\right]^{-1},$$

$$t_{d2}=\left[\cos(k_z h)-j\frac{\epsilon^2 k_{z0}^2+\epsilon_0^2 k_z^2}{2\epsilon\epsilon_0 k_{z0}k_z}\sin(k_z h)\right]^{-1},$$

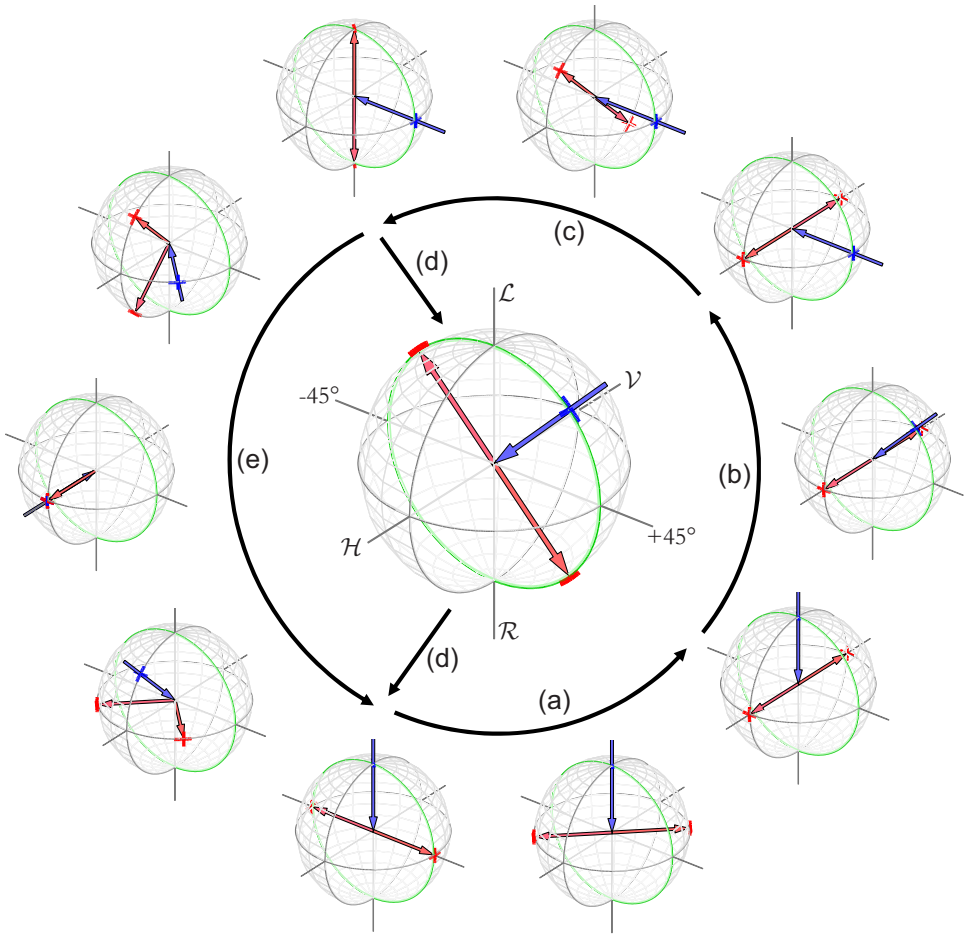

Fig. 6. (Color online) Illustration of the PCS device on the Poincaré sphere. The arrow with its head just at the center of the sphere denotes the incident polarization, while the two arrows pointing away from the center show the reflected and transmitted polarizations. The circle passing through $\mathcal{P}+45°$, $\mathcal{L}$, $\mathcal{P}-45°$, and $\mathcal{R}$ shows the polarizations aligned to the PBS axes, as in Eq. (13). Note that for the case when the incident polarization is aligned to the PBS, the arrows denoting the transmission and reflection polarizations are always antiparallel to each other and orthogonal to the arrow depicting the incidence polarization, showing that the incident polarization is separated into its two orthogonal constituents. The paths show what happens when some of the parameters are changed gradually, summarizing the operation of this type of PBS. (a) β changes from 0 to $\frac{1}{2}$ to 1 for the incidence polarization fixed at $\mathcal{L}$. (b) Incidence polarization changes from $\mathcal{L}$ to elliptical to $\mathcal{P}+45°$, for β fixed at 1. (c) β changes from 1 to $\frac{1}{2}$ to 0 for the incidence polarization fixed at $\mathcal{P}+45°$. (d) Incidence polarization changes from $\mathcal{P}+45°$ to elliptical to $\mathcal{L}$ for β fixed at 0. (e) The incident polarization is misaligned, rotating between the $\mathcal{P}+45°$ and $\mathcal{H}$ polarizations, and then between $\mathcal{H}$ and $\mathcal{L}$ polarizations.

$$r_{d1} = \left[j \frac{k_{z0}^2 - k_z^2}{2k_{z0}k_z} \sin(k_z h) \right] t_{d1},$$

$$r_{d2} = \left[j \frac{-\epsilon^2 k_{z0}^2 + \epsilon_0^2 k_z^2}{2\epsilon\epsilon_0 k_{z0}k_z} \sin(k_z h) \right] t_{d2}, \tag{20}$$

where $k_{z0} = \sqrt{\epsilon_0 \omega^2/c^2 - k_\parallel^2}$ and $k_z = \sqrt{\epsilon \omega^2/c^2 - k_\parallel^2}$ represent the wave vector components normal to the slab and $k_\parallel$ represents the wave vector component parallel to the slab. The other conditions are the same as in Sections 2 and 3: the PCS is surrounded by a medium with a dielectric constant of ϵ_0 (usually air/vacuum with $\epsilon_0 = 1$), and ϵ is the frequency-dependent dielectric constant fitted to the background.

Since the direct transmission and reflection coefficients corresponding to the polarizations 1 and 2 are in general different, the amplitude and phase responses will have a more complex form. More specifically, we will have two

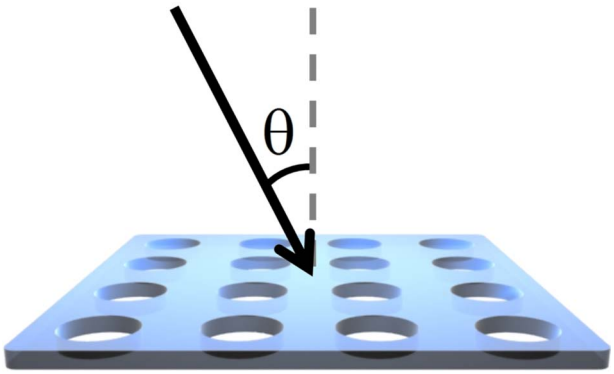

Fig. 7. (Color online) Illustration showing light incident on a PCS at an oblique angle. The azimuthal orientation of the incidence plane is irrelevant.

splitting ratios β_1 and β_2, defined as before through $r_{d1,2} = j\beta_{1,2}t_{d1,2}$. We can reduce this complexity by noting

$$\frac{\beta_2}{\beta_1} = 1 - \frac{k_\parallel^2}{\omega^2/c^2}\frac{\epsilon + \epsilon_0}{\epsilon\epsilon_0}. \tag{21}$$

By substituting $k_\parallel = \sqrt{\epsilon_0}(\omega/c)\sin\theta$, where θ is the incidence angle, and $\sqrt{\epsilon/(\epsilon+\epsilon_0)} = \sin\theta_{br}$, where θ_{br} is the Brewster angle [38], this ratio becomes

$$\frac{\beta_2}{\beta_1} = 1 - \frac{\sin^2\theta}{\sin^2\theta_{br}} = f. \tag{22}$$

For notational simplicity and clarity in further calculations, we will therefore write $\beta_1 = \beta$ and $\beta_2 = f\beta$, so that instead of two different splitting ratios, we have a single splitting ratio β and a simple function f dependent only on the angle of incidence.

We will now look for solutions satisfying the amplitude and orthogonality conditions as in Section 3, so that the PCS operates as a PBS under oblique incidence. The retardance for transmission will be, using Eq. (6),

$$\Delta\Phi_t = \arg(t_{d2}/t_{d1}) + \Phi_0 + \arg(\rho_t). \tag{23}$$

The phase parameter in this case is $\rho_t = (\alpha_2 \mp f\beta)(\alpha_1 \mp \beta)$. Because of the different direct transmission coefficients for the two polarizations, the retardance contains the additional phase contribution $\arg(t_{d2}/t_{d1})$. Similarly for the reflected wave, we have an additional phase contribution $\arg(r_{d2}/r_{d1})$. Hence, the retardance for reflection is

$$\Delta\Phi_r = \arg(r_{d2}/r_{d1}) + \Phi_0 + \arg(\rho_r). \tag{24}$$

The phase parameter for reflection in this case is $\rho_r = (1 \pm f\beta\alpha_2)(1 \pm \beta\alpha_1)$.

The amplitude condition for this oblique case is satisfied by these newly defined parameters in the same way as presented in the analysis leading from Eqs. (14) and (16) in Section 3, so that we obtain the two solutions presented in Eq. (16) for the oblique incidence case also, namely $\rho_r = -\rho_t$ and $\rho_r = +\rho_t$.

To satisfy the orthogonality condition in Eq. (17), we need to have $\Delta\Phi_r - \Delta\Phi_t = \arg(f\beta/\beta) + \arg(\rho_r/\rho_t) = \pi$. Since

$$\arg(f) = \arg\left(1 - \frac{\sin^2\theta}{\sin^2\theta_{br}}\right) = \begin{cases} 0 & \theta \leqslant \theta_{br} \\ \pi & \theta > \theta_{br} \end{cases}, \tag{25}$$

we should have $\rho_r = -\rho_t$ for $\theta \leqslant \theta_{br}$ and $\rho_r = +\rho_t$ for $\theta > \theta_{br}$. Solving $\rho_r = -\rho_t$, which corresponds to the case of $\theta \leqslant \theta_{br}$, we obtain the result

$$\omega^{(1)} = \omega_0 - \sqrt{\Delta^2 - \gamma^2 \mp 2\beta\Delta\gamma\frac{1-f}{1+f\beta^2}},$$

$$\omega^{(2)} = \omega_0 + \sqrt{\Delta^2 - \gamma^2 \mp 2\beta\Delta\gamma\frac{1-f}{1+f\beta^2}}. \tag{26}$$

Compared to the solution for normal incidence Eq. (18), this result is more general and includes an additional term that accounts for the effects of oblique incidence. The additional term is dependent on the background, in contrast to the normal incidence case. However, when there is a transmission peak in the Fabry–Perot type background spectrum at ω_0, i.e., no direct reflection corresponding to $\beta = 0$, our result reduces to

$$\omega^{(1)} = \omega_0 - \sqrt{\Delta^2 - \gamma^2},$$

$$\omega^{(2)} = \omega_0 + \sqrt{\Delta^2 - \gamma^2}. \tag{27}$$

This is the same result as the normal incidence case Eq. (18), independent of the angle of incidence.

Another implication of the additional term in Eq. (26) is that the splitting can be smaller than the linewidth, i.e., we can have $\Delta < \gamma$, depending on the angle of incidence and splitting ratio β. The effect of this additional parameter is insignificant for small angles, but can be more pronounced for angles close to the Brewster angle ($\theta \approx \theta_{br}$). At these angles, the splitting is allowed to be particularly small compared to the linewidth. If we then solve Eq. (26) at $\theta \approx \theta_{br}$ for the minimum splitting that will allow PBS operation, we obtain

$$\Delta_{min} = \gamma(\sqrt{\beta^2 + 1} \pm \beta). \tag{28}$$

We need to note that according to Eq. (26), we can have a splitting smaller than the linewidth only for the case of $\beta < 0$ for even modes and $\beta > 0$ for odd modes. For large $|\beta|$ Eq. (28) becomes $\Delta_{\min} = \frac{1}{2}\gamma/|\beta|$.

This means the two guided resonances do not have to be separated by as much compared to the normal incidence case, the amount of the splitting depending on how large the splitting ratio $|\beta|$ is, i.e., how high the direct reflection is. For a silicon PCS, however, the maximum $|\beta|$ is not very large. The highest theoretical reflection from a silicon mirror (half-wave thickness) is 72%. This corresponds to $|\beta| = 1.6$. Hence, the maximum $|\beta|$ possible for a silicon PCS is lower than 1.6. This means [Eq. (28)] that $\Delta_{min} = 0.29\gamma$. Hence, for angles of incidence not larger than the Brewster angle ($\theta \leqslant \theta_{br}$), a splitting of at least 0.29γ is necessary in a silicon PCS to use it as a PBS. For incidence angles larger than the Brewster angle ($\theta > \theta_{br}$), the requirements for the minimum splitting are quite different.

When we solve $\rho_r = +\rho_t$, which corresponds to the case of $\theta > \theta_{br}$, we obtain the result

$$\omega^{(1)} = \omega_0 \pm \beta\gamma\frac{1+f}{1-f\beta^2} - \sqrt{\Delta^2 + \gamma^2 + \left(\beta\gamma\frac{1+f}{1-f\beta^2}\right)^2},$$

$$\omega^{(2)} = \omega_0 \pm \beta\gamma\frac{1+f}{1-f\beta^2} + \sqrt{\Delta^2 + \gamma^2 + \left(\beta\gamma\frac{1+f}{1-f\beta^2}\right)^2}. \tag{29}$$

Similar to the previous case, when there is a transmission peak in the background spectrum at ω_0—i.e., no direct reflection, which corresponds to $\beta = 0$—our result reduces to the simple

$$\omega^{(1)} = \omega_0 - \sqrt{\Delta^2 + \gamma^2},$$

$$\omega^{(2)} = \omega_0 + \sqrt{\Delta^2 + \gamma^2}. \tag{30}$$

This result is very interesting, in that it allows solutions for $\Delta = 0$. In that case, the solutions are $\omega^{(1)} = \omega_0 - \gamma$ and $\omega^{(2)} = \omega_0 + \gamma$. For this case, at either side slope of a guided

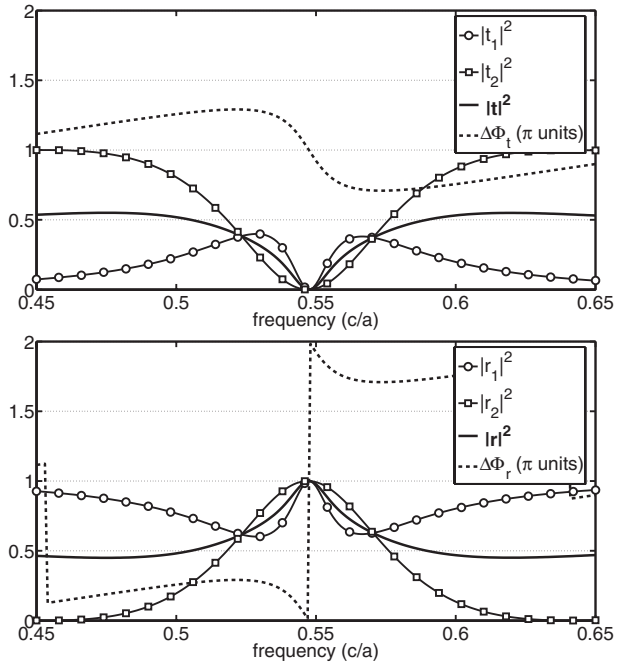

Fig. 8. Calculated spectra of the phase and amplitude responses for transmission (top) and reflection (bottom) for an oblique incidence angle larger than the Brewster angle, $\theta > \theta_{br}$ ($\theta = 80°$ and $\theta_{br} \approx 74°$) for the case of $\beta = 0$. The structural parameters of the PCS are the same as the ones used for Fig. 4. The guided resonances possess a half-linewidth of $\gamma = 0.040(2\pi c/a)$. The PBS frequencies are $\omega^{(1)} = 0.51(2\pi c/a)$ and $\omega^{(2)} = 0.59(2\pi c/a)$, respectively.

resonance, the PCS will act as a PBS. Note that we can also have $\Delta = 0$ for other β values, as long as $\theta > \theta_{br}$. A plot verifying Eq. (30) for $\Delta = 0$ is shown in Fig. 8. The calculations were carried out by directly using the basic expressions in Eqs. (1) and (20).

It is interesting how the Brewster angle is involved in the mechanisms behind PBS operation of a PCS. The Brewster angle in this case serves as a boundary, merely separating two ranges of angles ($\theta \leqslant \theta_{br}$ and $\theta > \theta_{br}$) that affect the PCS differently in separating an incoming beam into its orthogonal constituents. This is in contrast to standard PBS or polarizer applications, where the Brewster angle itself is directly relevant ($\theta = \theta_{br}$) to the mechanism of polarizing and beam splitting.

5. RESULTS

Here we present results of an FDTD simulation for a circular PBS device (Fig. 9) and some experimental data on a fabricated structure [scanning-electron-microscope image (SEM) shown in Fig. 10)].

Figure 9 shows FDTD results for a PCS structure acting as a circular PBS. The simulations were done for a plane wave that was linearly polarized at 45° incident on a form-birefringent PCS. The spectra are normalized with respect to an incident wave spectrum calculated in an identical simulation without the PCS present. To obtain the normalized reflection spectrum, the incident wave data are subtracted from the reflected wave before normalization. The phase is calculated directly from the complex wave amplitude. The simulated PCS structure was

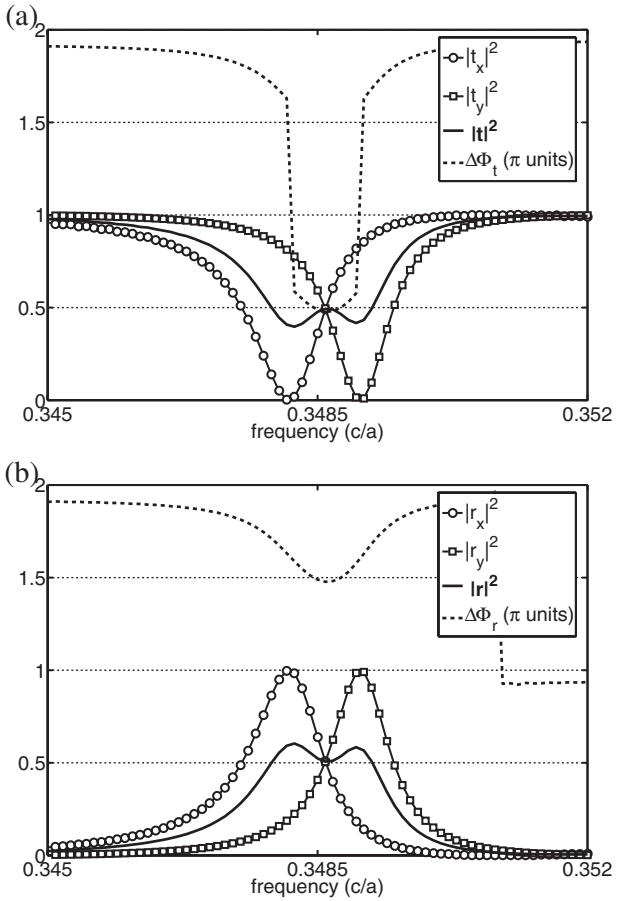

Fig. 9. FDTD simulations showing (a) transmission results and (b) reflection results for a circular PBS.

designed through the method described in Appendix A. This particular structure has a dielectric constant of 12 (which roughly corresponds to the dielectric constant of Si or GaAs at optical wavelengths) and a thickness of $h = 0.85a$. The form birefringence is due to the capsule-shaped holes illustrated in Fig. 11. We prefer this shape in generating form birefringence over elliptical holes (or different lattice constants in the two directions) because

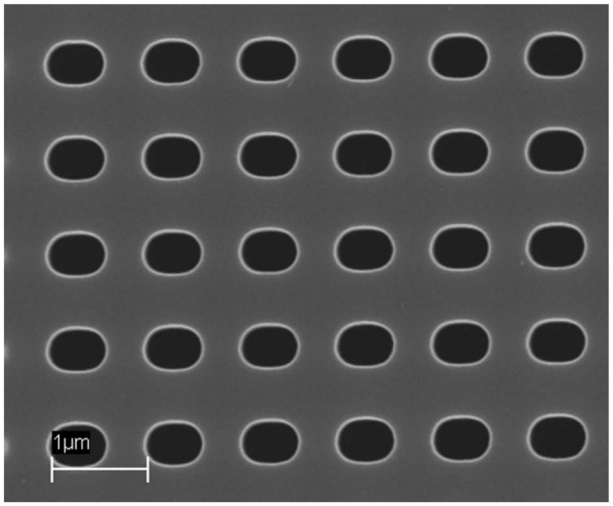

Fig. 10. SEM image of a fabricated sample with capsule shaped holes on a silicon slab.

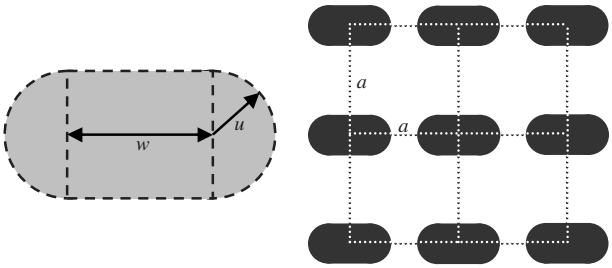

Fig. 11. Capsule-shaped holes. The shape defined by two parameters, the rectangle width w and semicircle radius u, is responsible for the form birefringence in the PCS.

of its simplicity in simulations and fabrication. The capsule shape is built up of a rectangle with semicircles on each end, hence is defined by two parameters, the rectangle width w and semicircle radius u. The parameters for the holes used in the simulation are $w=0.35a$ and $u=0.1a$. The ω_0 frequency for these split guided resonances is 0.3485 $(2\pi c/a)$ with a linewidth of 0.0010 $(2\pi c/a)$. We clearly see that the phase and amplitude responses have the behavior predicted by our analysis in Section 2. Such simulation results provide parameters for real devices that we can fabricate. The single-dielectric nature of such a structure makes it relatively easy to fabricate through lithography techniques. Below we describe how we fabricate some simple structures on silicon.

The starting material for fabrication of the PCS device shown in Fig. 10 is silicon-on-insulator wafers with (100) crystal orientation. To create 100 μm $\times$ 100 μm free-standing silicon membranes, we patterned 808 μm wide square apertures on the back of the wafers and used 30% KOH in water to etch through the 500 μm thick substrate. For defining the holes, we employ an electron-beam lithography tool and plasma etching. The size of individual crystals is 100 μm $\times$ 100 μm, matching the size of the KOH etched diaphragms. The final PCS structure has a slab thickness of 450 nm. The capsule-shaped holes have the parameters $w=125$ nm and $u=250$ nm and are on a square lattice with a lattice constant of $a=1000$ nm.

After fabrication, the devices are characterized in a simple measurement setup. To measure the transmission spectrum of the structures, we use a broadband light source that emits spatially coherent light through a single-mode fiber in the wavelength range 1300–1600 nm. A linear rotating polarizer is placed in front of the fiber output, which illuminates the PCS. The core of the fiber is imaged by a microscope objective with a magnification of 5 onto the PCS, giving an illumination spot with a diameter equal to 50 μm, 5 times the 10 μm fiber mode diameter. The microscope objective used in the setup has a numerical aperture of 0.1 and a rear conjugate at 160 mm, where the PCS is placed and illuminated at normal incidence. The transmitted light is picked up by an identical microscope objective that demagnifies the spot onto a single-mode fiber, which is connected to an optical spectrum analyzer. The diameter of the spot on the PCS that is captured by the single-mode fiber is $\approx$50 μm, 5 times the 10 μm fiber mode diameter; hence it falls well within the area of the PCS.

Figure 12(a) shows the measured transmission for the two polarizations for a structure with $\beta\approx 0$ at $\omega=\omega_0$. We see that the two resonances are separated by one linewidth. To test the quarter-wave retardation [Fig. 12(b)] in the vicinity of the center frequency, we first measure the spectrum of the PCS structure by illuminating it with linearly polarized light (polarization plane at 45°), obtaining the average of the spectra of Fig. 12(a). Then we place a quarter-wave plate followed by a linear polarizer (polarization plane at 45°) after the PCS structure with the fast and slow axes aligned to the PCS. For ideal conditions, the drop in transmission at the center frequency with the quarter-wave plate present should be 100%. We observe a 60% drop in transmission instead, suggesting some ellipticity in the polarization, but showing the principle of operation that by splitting the guided resonances through an introduction of form birefringence turns the PCS into a retarder. We also have characterized a sample with $\beta\approx -1$ at $\omega=\omega_0$ that acts as a linear PBS (Fig. 13).

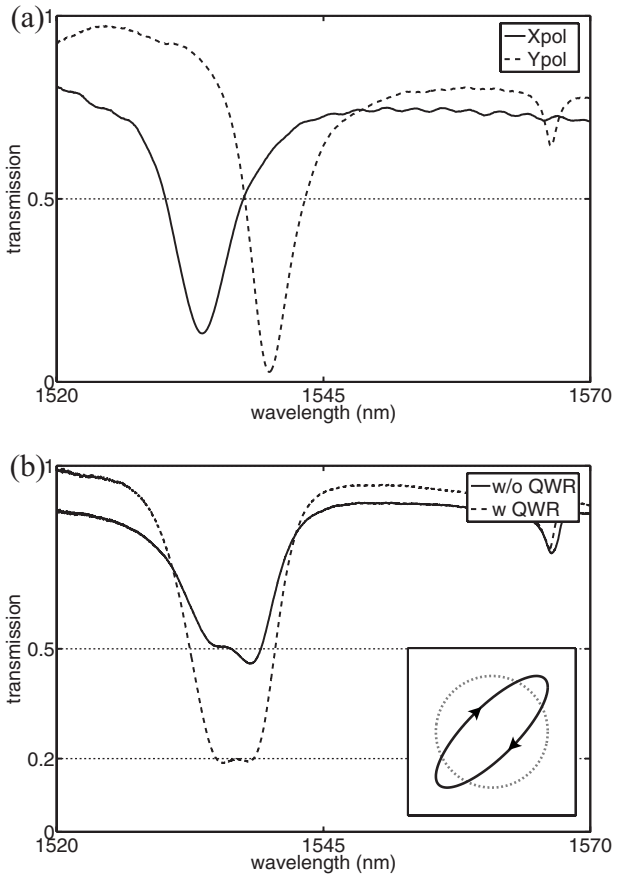

Fig. 12. (a) Experimental results showing two guided resonances corresponding to two different polarizations that are separated by one linewidth. This corresponds to $\beta\approx 0$. (b) Experimental results showing the transmission spectrum for the PCS that is illuminated with linearly polarized light at 45° (solid curve). As expected, the spectrum is the average of the two spectra in (a). When we put a quarter-wave plate followed by a linear polarizer at 45° after the PCS, we observe a drop in the transmission (dashed curve). For ideal conditions, the drop in the transmission at the center frequency should be 100%. Here, however, we observe a 60% drop in transmission, suggesting some ellipticity in the polarization. The inset shows the polarization state of the transmitted light calculated from these measurement data. Compared with the ideal case, a circular polarization state (shown as a dotted circle in the inset), we clearly see that there is a significant amount of ellipticity in the transmitted light.

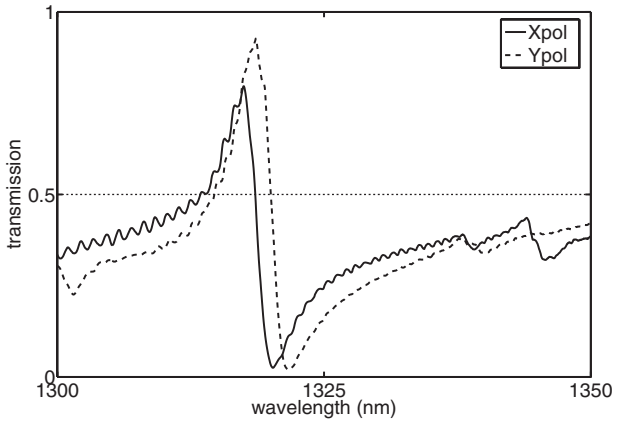

Fig. 13. Experimental results showing two guided resonances corresponding to two different polarizations that are separated by one linewidth. This corresponds to a linear PBS with $\beta \approx -1$.

6. DISCUSSIONS

The analysis we have provided in Sections 2–4, together with the results consistent with this analysis that we have presented in Section 5, show that the PCS structure we describe is feasible for real applications. Besides regular PBS applications, this structure can be employed in polarization control in vertical cavity surface-emitting lasers, and can be used as a key element in various optical interconnection schemes. The PCS-based PBS is especially suitable for the latter applications due to the single dielectric nature of the structure and its tunability through simple geometrical parameters that can be arbitrarily defined in a single lithography step.

There are several limitations of such PBS structures that can constitute obstacles depending on the application. Let us analyze the limitations of the structures that were reported in [3] for this type of PBS application. First, the structure possesses chromaticity. The wavelength range $\Delta\lambda$ where the PCS structure acts as a PBS is determined mainly by γ, i.e., the linewidth of the guided resonance. For a typical Q value range for guided resonances of $\approx$100 to $\approx$5000 [29], the operation bandwidth ranges from 0.3 nm to 15 nm at telecom wavelengths ($\approx$1500 nm). Note, however, that the diattenuation varies faster (see, e.g., Fig. 4). That means, although in the bandwidth $\Delta\omega = \gamma$ the incoming light is separated into two orthogonal polarizations, the respective powers in the two polarizations vary over that frequency range. This means that the reflected and transmitted waves remain orthogonal over that range, but the polarization varies, such as from linear to circular.

For a large bandwidth, a large linewidth is preferred. However, a large linewidth corresponds to a small Q factor. And as we discussed in Section 3, we made our analysis with the assumption that the Q factors of guided resonances are typically large. At this point we need to ask the question, How small can Q be to have an efficient PBS operation? To find an answer to this, we need to consider the relative changes in the linewidths when two resonances are split by the order of one linewidth. When the two resonances split, their linewidths will change by a small amount $\delta\gamma$ so that the resonance with the lower frequency acquires a linewidth decreased by this amount, and that with the higher frequency acquires a linewidth increased by this amount. We showed that $\delta\gamma/\gamma$ is of the order of $1/Q$, which was the reason that we considered it insignificant for high-Q resonances. Using the expressions provided by the analysis in Section 3, we find the interesting result that the equal-power condition $\mathrm{Tr}(J_t^\dagger J_t) = \mathrm{Tr}(J_r^\dagger J_r)$ and the orthogonality condition $\mathrm{Tr}(J_t^\dagger J_r) = 0$ are still satisfied to the first order of $\delta\gamma/\gamma$. Further analysis yields the result that there is a higher-order dependence on $\delta\gamma/\gamma$, so that we have approximately $\mathrm{Tr}(J_t^\dagger J_t) - \mathrm{Tr}(J_r^\dagger J_r) \approx 1/Q^2$ and $\mathrm{Tr}(J_t^\dagger J_r) \approx 1/Q^3$.

Therefore, the conditions for attainment of a PBS even hold for Q values that are smaller than we assumed in the first place. Hence, the orthogonal and equal-power splitting properties of the structure are robust to first-order variations in the linewidth. The diattenuation D, on the other hand, can change by amounts of this order. It turns out that $D = \delta\gamma/\gamma$ for $\beta = 0$, and $D = 1$ for $\beta = \pm 1$. Therefore, a circular PBS becomes slightly elliptical, while a linear PBS is not affected to this order. These effects on the diattenuation, however, can be compensated for by changing ω_0 slightly during design, so that the resonances reside on slightly different background values.

Some simple applications employing a PCS-based PBS at normal incidence and oblique incidence are illustrated in Fig. 14. The first illustration [Fig. 14(a)] shows a Gires–Tournois configuration [39]. By changing the distance between the mirror and the PCS, it is possible to control the polarization state of the output beam. In fact, this configuration allows a full phase difference between 0 and π. Such a device can be used as a mirror in a laser cavity enabling dynamic polarization control. The second illustration [Fig. 14(b)] shows how to use a PCS-PBS for sensor applications. The PCS-based QWR can be designed to be highly chromatic, normally a disadvantage for a QWR, by employing high-Q guided resonances. In such a case, a slight change in the PCS background, such as through heat, mechanical stress, etc., will destroy the orthogonality in the polarizations of the transmitted and reflected waves. For the configuration shown, one would then see interference in the output beam for any small effect on the PCS.

Another feature of such a detection scheme is that there is no cumbersome alignment requirement, even though it is based on two-beam interferometry. Also, in certain cases, sharp variation of polarization properties as a function of frequency can be advantageous. Employing a high-Q resonance may result in its utility for applications such as polarization mode dispersion.

APPENDIX A

Here we briefly present the design rules for a PBS based on a form-birefringent PCS operating at normal incidence, and which may also be used to design a PBS at oblique incidence. We demonstrated in Section 3 that the only condition for constructing such a PBS is to have a small amount of form birefringence so that two guided resonances corresponding to two different eigenpolarizations are separated by larger than one linewidth. We will consider the least dispersive solution, when the splitting equals the linewidth.

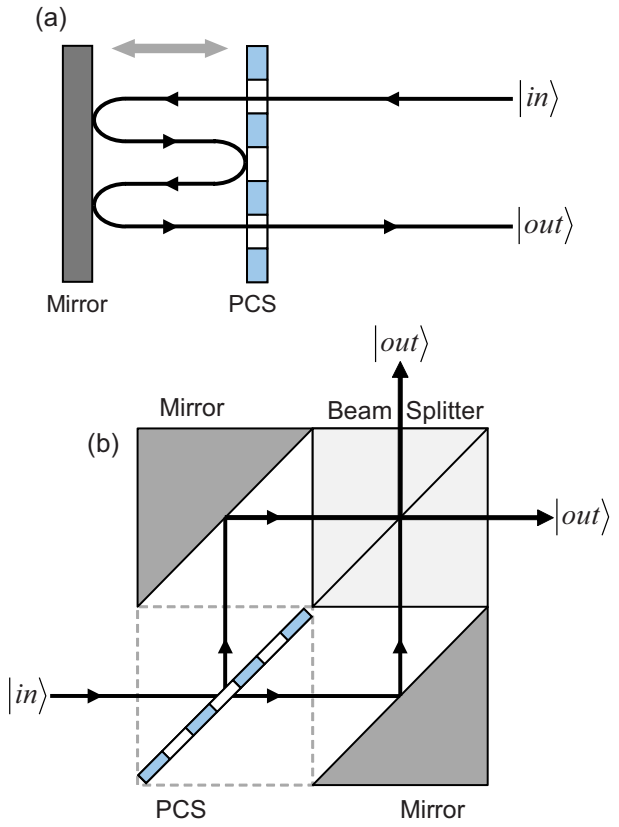

Fig. 14. (Color online) Some applications of the PCS structure. (a) The PCS-PBS structure in a Gires–Tournois configuration. By changing the distance between the mirror and the PCS, it is possible to control the polarization state of the output beam. Such a device can be used as a mirror in a laser cavity enabling dynamic polarization control. (b) The PCS can be designed to be highly chromatic, normally a disadvantage for QWRs. In such a case, a slight change in the PCS background, such as through heat, mechanical stress, etc., will destroy the orthogonality in the polarizations of the transmitted and reflected waves. For the configuration shown, one would then see interference in the output beam for any small effect on the PCS. The nice feature of such a detection scheme is that there is no cumbersome alignment requirement even though it is based on two-beam interferometry.

The form birefringence can be introduced into the lattice through, e.g., elliptical holes, or through different lattice constants in two directions. In such a case, guided resonances that are doubly degenerate for a symmetric crystal split into two, so that there are two distinct resonances for the two eigenpolarizations. The splitting can be controlled by the degree of ellipticity of the holes, or by the asymmetry of the lattice constants in two directions. That way the one-linewidth-separation condition can be satisfied at normal incidence. The design for such a structure can be done in the following steps.

First the design, i.e., the simulation, is done for a symmetric PCS. In the first step we decide on the type of beam splitter, i.e., on the value of β (at $\omega=\omega_0$). At normal incidence then, a guided resonance has to have one of the following frequencies, which are found through the definition of the splitting ratio $\beta(\omega)$ in Eq. (3):

$$\omega_m = \frac{1}{2\pi h\sqrt{\epsilon}}\left[\sin^{-1}\left(\frac{2\sqrt{\epsilon}}{1-\epsilon}\beta\right) + m\pi\right]$$

$$m = \ldots -2, -1, 0, 1, 2, \ldots, \quad \text{(A1)}$$

where we take only the positive frequency solutions. Here ω is in units of $2\pi(c/a)$, a being the lattice constant and c the speed of light; h is in units of a. If we want to construct a circular polarizer, for instance, we need to have $\beta=0$, so that

$$\omega_m = \frac{m}{2h\sqrt{\epsilon}} \qquad m = 1, 2, 3, \ldots . \quad \text{(A2)}$$

This actually means that for $\beta=0$, a guided resonance should be centered at a point where the background reflectivity vanishes, i.e., $|r_d|^2=0$. Similarly, for $\beta=\pm 1$, a guided resonance should be centered at a point where $|r_d|^2=|t_d|^2=1/2$.

In the second step, we do a simulation for a chosen h and u (radius of a circular hole). If a guided resonance is not at one of the ω_m frequencies, we change the u value. Increasing or decreasing u shifts the center frequency of a guided resonance into the positive or negative direction, respectively. (As we demonstrated, the center frequency changes faster than the linewidth and background.) We change u gradually until we have a resonance centered at a ω_m (i.e., a resonance where $|r_d|^2=0$ for a $\beta=0$ design).

In the final step, we split the doubly degenerate guided resonance (centered now at a ω_m) in two by breaking the 90° rotational symmetry. We can do it by introducing either elliptical holes or different lattice constants in two directions. We should change (u_1,u_2) for an ellipse, or (a_1,a_2) for an asymmetric pitch, in such a way that we keep the average dielectric constant the same. Therefore, for elliptical holes we should have $u_1\times u_2=u^2$ (or for a small difference Δu, $u_1=u-\Delta u$ and $u_2=u+\Delta u$). Similarly, for an asymmetric pitch we should have $a_1\times a_2=a^2$ (or for a small difference Δa, $a_1=a-\Delta a$ and $a_2=a+\Delta a$). The degree of asymmetry should be increased or decreased to achieve the one-linewidth-separation condition. This finishes the design, and due to the scalability of the system in terms of a, the design frequency can be translated into any physical frequency with an appropriate choice of a.

ACKNOWLEDGMENTS

The authors would like to acknowledge Wonjoo Suh and Zheng Wang for their assistance in the FDTD simulations. This work was sponsored by the U.S. Army Research Laboratory under contract DAAD17-02-C-0101.

REFERENCES AND NOTES

1. T. B. Pittman, B. C. Jacobs, and J. D. Franson, "Probabilistic quantum logic operations using polarizing beam splitters," Phys. Rev. A **64**, 062311 (2001).
2. P. Kok, C. P. Williams, and J. P. Dowling, "Construction of a quantum repeater with linear optics," Phys. Rev. A **68**, 022301 (2003).
3. J. L. Pezzaniti and R. A. Chipman, "Angular dependence of polarizing beam splitter cubes," Appl. Opt. **33**, 1916–1929 (1994).
4. D. Yi, Y. Yan, H. Liu, S. Lu, and G. Jin, "Broadband polarizing beam splitter based on the form birefringence of a subwavelength grating in the quasi-static domain," Opt. Lett. **29**, 754–756 (2004).
5. D. Dias, S. Stankovic, H. Haidner, L. L. Wang, T. Tschudi,

M. Ferstl, and R. Steingrüber, "High-frequency gratings for applications to DVD pickup systems," J. Opt. A, Pure Appl. Opt. **3**, 164–173 (2001).
6. M. C. Gupta and S. T. Peng, "Multifunction grating for signal detection of optical disk," Proc. SPIE **1499**, 303–306 (1991).
7. A. G. Lopez and H. G. Craighead, "Wave-plate polarizing beam splitter based on a form-birefringent multilayer grating," Opt. Lett. **23**, 1627–1629 (1998).
8. M. Schmitz, R. Brauer, and O. Bryngdahl, "Gratings in the resonance domain as polarizing beam splitters," Opt. Lett. **20**, 1830–1831 (1995).
9. R. C. Tyan, P. C. Sun, and Y. Fainman, "Polarizing beam splitters constructed of form-birefringent multilayer gratings," Proc. SPIE **2689**, 82–89 (1996).
10. R. C. Tyan, P. C. Sun, A. Scherer, and Y. Fainman, "Polarizing beam splitter based on anisotropic spectral reflectivity characteristics of form-birefringent multilayer gratings," Opt. Lett. **21**, 761–763 (1996).
11. G. R. Bird and M. Parrish, Jr., "The wire grid as a near-infrared polarizer," J. Opt. Soc. Am. **50**, 886–891 (1960).
12. R. Magnusson and S. S. Wang, "New principle for optical filters," Appl. Phys. Lett. **61**, 1022–1024 (1992).
13. J. R. Wendt, G. A. Vawter, R. E. Smith, and M. E. Warren, "Subwavelength, binary lenses at infrared wavelengths," J. Vac. Sci. Technol. B **15**, 2946–2949 (1997).
14. R. C. Enger and S. K. Case, "Optical elements with ultrahigh spatial-frequency surface corrugations," Appl. Opt. **22**, 3220–3228 (1983).
15. L. H. Cescato, E. Gluch, and N. Streibl, "Holographic quarter-wave plate," Appl. Opt. **29**, 3286–3290 (1990).
16. D. C. Flanders, "Submicrometer periodicity gratings as artificial anisotropic dielectrics," Appl. Phys. Lett. **42**, 492–494 (1983).
17. H. Kikuta, Y. Ohira, and K. Iwata, "Achromatic quarter-wave plates using the dispersion of form birefringence," Appl. Opt. **36**, 1566–1572 (1997).
18. G. P. Nordin and P. C. Deguzman, "Broadband form birefringent quarter-wave plate for the mid-infrared wavelength region," Opt. Express **5**, 163–168 (1999).
19. S. D. Jacobs, K. A. Cerqua, K. L. Marshall, A. Schmid, M. J. Guardalben, and K. J. Skerrett, "Liquid-crystal laser optics: design, fabrication, and performance," J. Opt. Soc. Am. B **5**, 1962–1979 (1988).
20. J. A. Davis, J. Adachi, C. R. Fernández-Pousa, and I. Moreno, "Polarization beam splitters using polarization diffraction gratings," Opt. Lett. **26**, 587–589 (2001).
21. R. M. A. Azzam and F. A. Mahmoud, "Symmetrically coated pellicle beam splitters for dual quarter-wave retardation in reflection and transmission," Appl. Opt. **41**, 235–238 (2002).
22. R. M. A. Azzam and A. De, "Circular polarization beam splitter that uses frustrated total internal reflection by an embedded symmetric achiral multilayer coating," Opt. Lett. **28**, 355–357 (2003).
23. D. R. Solli, C. F. McCormick, R. Y. Chiao, and J. M. Hickmann, "Photonic crystal polarizers and polarizing beam splitters," J. Appl. Phys. **93**, 9429–9431 (2003).
24. D. R. Solli, C. F. McCormick, R. Y. Chiao, and J. M. Hickmann, "Birefringence in two-dimensional bulk photonic crystals applied to the construction of quarter waveplates," Opt. Express **11**, 125–133 (2003).
25. V. Lousse, W. Suh, O. Kilic, S. Kim, O. Solgaard, and S. Fan, "Angular and polarization properties of a photonic crystal slab mirror," Opt. Express **12**, 1575–1582 (2004).
26. V. N. Astratov, I. S. Culshaw, R. M. Stevenson, D. M. Whittaker, M. S. Skolnick, T. F. Krauss, and R. M. D. L. Rue, "Resonant coupling of near-infrared radiation to photonic band structure waveguides," J. Lightwave Technol. **17**, 2050–2057 (1999).
27. M. Boroditsky, R. Vrijen, T. F. Krauss, R. Coccioli, R. Bhat, and E. Yablonovitch, "Spontaneous emission extraction and purcell enhancement from thin-film 2-D photonic crystals," J. Lightwave Technol. **17**, 2096–2112 (1999).
28. A. Erchak, D. J. Ripin, S. Fan, P. Rakich, J. D. Joannopoulos, E. P. Ippen, G. S. Petrich, and L. A. Kolodziejski, "Enhanced coupling to vertical radiation using a 2D photonic crystal in a semiconductor LED," Appl. Phys. Lett. **78**, 563–565 (2001).
29. S. Fan and J. D. Joannopoulos, "Analysis of guided resonances in photonic crystal slabs," Phys. Rev. B **65**, 235112 (2002).
30. S. Fan, W. Suh, and J. D. Joannopoulos, "Temporal coupled-mode theory for the Fano resonance in optical resonators," J. Opt. Soc. Am. A **20**, 569–572 (2003).
31. M. Kanskar, P. Paddon, V. Pacradouni, R. Morin, A. Busch, J. F. Young, S. R. Johnson, J. Mackenzie, and T. Tiedje, "Observation of leaky slab modes in an air-bridged semiconductor waveguide with a two-dimensional photonic lattice," Appl. Phys. Lett. **70**, 1438–1440 (1997).
32. M. Meier, A. Mekis, A. Dodabalapur, A. A. Timko, R. E. Slusher, J. D. Joannopoulos, and O. Nalamasu, "Laser action from two-dimensional distributed feedback in photonic crystals," Appl. Phys. Lett. **74**, 7–9 (1999).
33. S. Noda, M. Yokoyama, M. Imada, A. Chutinan, and M. Mochizuki, "Polarization mode control of two-dimensional photonic crystal laser by unit cell structure design," Science **293**, 1123–1125 (2001).
34. H. Y. Ryu, Y. H. Lee, R. L. Sellin, and D. Bimberg, "Over 30-fold enhancement of light extraction from free-standing photonic crystal slabs with InGaAs quantum dots at low temperature," Appl. Phys. Lett. **79**, 3573–3575 (2001).
35. P. Yeh, *Optical Waves in Layered Media* (Wiley, 1988).
36. K. Sakoda, *Optical Properties of Photonic Crystals* (Springer-Verlag, 2001).
37. For a complex number $z=|z|e^{j\Phi}$, the phase will be $\Phi=\arg(z)$. We restrict the phase to the principal value, so that $-\pi<\arg(z)\leqslant\pi$. The argument of a complex number has the properties $\arg(z_1)+\arg(z_2)=\arg(z_1z_2)$, and $\arg(z_1)-\arg(z_2)=\arg(z_1/z_2)$. The argument of a real number $\arg(R)$ will be 0 and π for $R\geqslant 0$ and $R<0$, respectively.
38. E. Hecht, *Optics* (Addison-Wesley, 1998).
39. F. Gires and P. Tournois, "Interféromètre utilisable pour la compression d'impulsions lumineuses modulées en fréquence," C. R. Acad. Sci. Paris **258**, 6112–6115 (1964).